Acta Crystallographica Section B
Structural Science
ISSN 0108-7681

Characterization of the room-temperature phase of Tl_2MoO_4: crystal structure, symmetry mode analysis and second-harmonic generation measurements

Karen Friese,[a]* Mois I. Aroyo,[a] Cesar L. Folcia,[a] Gotzon Madariaga[a] and Tomasz Breczewski[b]

[a]Departamento de Física de la Materia Condensada, Universidad del País Vasco, Apdo. 644, Bilbao, Spain, and [b]Departamento de Física Aplicada II, Universidad del País Vasco, Apdo. 644, Bilbao, Spain

Correspondence e-mail: wmbfrxxk@lg.ehu.es

Received 3 July 2000
Accepted 27 October 2000

The crystal structure of the glaserite-related compound dithallium(I)–molybdate(VI), which at 293 K crystallizes monoclinic, space group $C121$ with lattice parameters a = 10.565 (3), b = 6.418 (1), c = 8.039 (2) Å, β = 91.05 (4)°, has been determined. The structure was refined as an inversion twin to a final $R(F_{all})$ value of 0.0611 for 1006 unique reflections [$R(F_{obs})$ = 0.0285 for 644 observed reflections]. Second-harmonic generation measurements led to a value of d_{eff} = 5.5 ± 0.5 pm V^{-1} as an estimation of the second-harmonic conversion efficiency at phase matching. Symmetry mode analysis shows that, in general, primary modes have the highest amplitudes, yet surprisingly some of the secondary modes assume amplitudes of comparable magnitude. A comparison of the phase at 293 K with that at 350 K (space group $P\bar{3}m1$) shows that the main change can be described as a rotation of the molybdate tetrahedra around the trigonal $a(b)$ axis. The molybdate tetrahedra as well as the octahedra around one of the symmetry-independent Tl atoms are more strongly distorted in the monoclinic phase. The coordination number for the other two Tl atoms is decreased from 12 and 10 in the high-symmetry phase to 10 and 9 in the monoclinic phase. Furthermore, the number of common edges between the Tl and Mo coordination polyhedra is reduced and the common face which is observed between them in the high-temperature phase is changed to a common edge in the low-temperature phase. The contribution of the primary symmetry modes leads exactly to this change in the coordination spheres of the atoms.

1. Introduction

A series of compounds assuming the glaserite-type structure have been characterized in the literature so far. The structure of the mineral glaserite $NaK_3(SO_4)_2$ is characterized by isolated $[SO_4]^{6-}$ tetrahedra alternating with three different polyhedra of coordination number 6, 10 and 12 which are formed around the monovalent cations. The structure has been described in detail by *e.g.* Moore (1973). The ideal glaserite structure belongs to the space group $P\bar{3}m1$, yet related compounds are known which assume lower monoclinic symmetry ($C2/c$ or $C2/m$). Lattice parameters of some selected compounds are given in Table 1. In the glaserite-related structures the three non-equivalent positions for the monovalent cations are generally occupied by two different species, depending on the sizes of the cavities and the cations, respectively. Anyhow, in some cases the same species of monovalent cation is found in the three different coordination polyhedra, *e.g.* Tl_2WO_4 (Okada & Ossaka, 1979) and Tl_2MoO_4 (Friese *et al.*, 1999).

Phase transitions have been observed for a couple of compounds which are isotypical to glaserite. However, only in two cases [$K_3Na(SeO_4)_2$ and $K_3Na(CrO_4)_2$] have the structures of the different phases involved been successfully refined. These two compounds undergo a structural phase transition from $P\bar{3}m$ to $C2/c$ (with a doubled c parameter).

According to van den Akker (1970), each of the four compounds K_2MoO_4, Rb_2MoO_4, K_2WO_4 and Rb_2WO_4 undergo two phase transitions. The transition sequence proposed for them is

$$P\bar{3}m1 \longrightarrow \text{orthorhombic phase } (\beta - K_2SO_4?) \longrightarrow C2/m.$$

Of these compounds only the structures of the $C2/m$ phase have been characterized by single-crystal X-ray diffraction, while detailed information about the orthorhombic and trigonal phases are still missing. Furthermore, for the orthorhombic phases of the potassium salts and rubidium tungstate the authors report the existence of unindexable lines in the powder diffraction patterns which, according to van den Berg *et al.* (1973), can be interpreted assuming the presence of satellite reflections, thus indicating the existence of modulated structures. van den Berg *et al.* (1983) were able to refine the average structure of the orthorhombic phase (space group *Ccmm*) of K_2MoO_4, yet due to experimental difficulties they could not take into account the satellite reflections and perform a complete analysis in higher-dimensional space.

For Tl_2WO_4 three different phase transitions have been observed at 835, 310 and 283 K (Sleight *et al.*, 1975). The authors proposed the following sequence of space groups

$$P6_3/mmc \longrightarrow ??? \longrightarrow P\bar{3}m1 \longrightarrow Pna2_1.$$

Of these phases only the structure at room temperature is known and was successfully refined in the space group $P\bar{3}m1$ by Okada & Ossaka (1979).

A contradiction exists as to the number of phase transitions in Tl_2MoO_4. Three phase transitions have been reported by Gaultier & Pannetier (1972) at 776, 673 and 311 K, respectively. Sleight *et al.* (1975) reaffirmed the phase transitions at 776 and 311 K, but they could not detect any at 673 K. Both authors agree that the structure at room temperature is orthorhombic and that the intermediate phase above 311 K crystallizes trigonal with space group $P\bar{3}m1$. We refined the structure of Tl_2MoO_4 at 350 K and could show that it really assumes the trigonal space group $P\bar{3}m1$ and is isotypical to glaserite (Friese *et al.*, 1999).

The aim of the present work was to characterize the room-temperature phase, which according to Gaultier & Pannetier (1972) assumes the orthorhombic space group *Pnam* with lattice parameters a = 7.919 (5), b = 11.026 (7) and c = 6.179 (5) Å. According to Sleight *et al.* (1975), on the other hand, the structure is noncentrosymmetric with comparable lattice parameters and assumes the space group $Pna2_1$.

2. Optical measurements

The relatively strong second-harmonic generation (SHG) signal observed in a polycrystalline sample of Tl_2MoO_4 suggested to try a quantitative characterization of this material. Yet, as can easily be observed in an optical microscope, the phase transition of Tl_2MoO_4 at 311 K is accompanied by the appearance of multiple domains below the transition temperature. This fact was the main obstacle in the measurements and forced us to use an extremely small sample, which appeared to consist of one single domain only.

SHG measurements were carried out using a Q-switched Nd^{3+}:YAG laser (wavelength λ = 1064 nm, pulse width 6 ns, pulse frequency 5 Hz). The pulse energy was 0.8 mJ and the intensity at the sample was 6.7 MW cm^{-2}. The complete experimental setup has been described elsewhere (Pereda *et al.*, 1998). For the present study a single domain hexagonal prismatic crystal of Tl_2MoO_4 with the area 0.0125 ± 0.0005 mm^2 and thickness $d = 3 \pm 0.5$ µm was selected. The crystal was held between a microscope slide and a cover glass joined with oil.

X-ray diffraction experiments (see §3) demonstrate that the point group of Tl_2MoO_4 is monoclinic. The two extinction directions, one corresponding to the twofold axis, could be clearly observed with a polarizing microscope. According to the symmetry of the second-order susceptibility tensor which describes SHG for point group 2, the second harmonic field is polarized along the twofold axis when the fundamental wave is polarized parallel or perpendicular to it. Thus, the direction of the twofold axis was determined from the polarization state of the second harmonic light.

The measurements were performed in the so-called type I phase-matching experimental configuration: second harmonic light was detected as a function of incidence while the sample was rotated about the twofold axis (vertical) direction and the fundamental wave was horizontally polarized. The SHG conversion efficiency $d_{\rm eff}$ is

$$d_{\rm eff} = d_{21}\cos^2\theta + d_{23}\sin^2\theta - 2d_{25}\sin\theta\cos\theta, \qquad (1)$$

where θ is the refraction angle inside the material and d_{ij} are the second-order susceptibility coefficients. Here the d_{ij} tensor is referred to a coordinate system in which z is oriented along the crystal plate normal and y is parallel to the twofold axis. The angular dependence of the second harmonic power is given by Yariv & Yeh (1984)

$$P^{2\omega} = \frac{8\omega^2 d_{\rm eff}^2 L^2 (t^{\omega})^4 (t^{2\omega})^2}{\epsilon_0 c^3 n^3 A}\left[\frac{\sin(\frac{\Delta KL}{2})}{(\frac{\Delta KL}{2})}\right]^2 (P^{\omega})^2, \qquad (2)$$

where $L = d/\cos\theta$ is the interaction length, A and P^{ω} are the effective sample area and the resultant incidence power, respectively, t^{ω} and $t^{2\omega}$ are Fresnel transmission factors and n is the refractive index of the material. As it is extremely difficult to measure a refractive index higher than 1.7 with a reasonable degree of accuracy, we estimated n using the Gladstone–Dale relationship (Mandarino, 1976, 1978; $n \simeq 2$). $\Delta K = (4\pi/\lambda)[n_v^{2\omega} - n_h^{\omega}(\theta)]$, where $n_h^{\omega}(\theta)$ is the angular-dependent refractive index of the fundamental field with frequency ω, and $n_v^{2\omega}$ is the (constant) refractive index for the vertically polarized second harmonic wave. Thus, a maximum in $P^{2\omega}$ occurs if

Table 1
Lattice parameter of glaserite-related compounds.

Compound	a (Å)	b (Å)	c (Å)	β (°)	Reference
Space group $P\bar{3}m1$					
$NaRb_3(BeF_4)_2$	5.805	5.805	7.556		Pontonnier *et al.* (1972)
$NaK_3(SO_4)_2$	5.6801 (6)	5.6801 (6)	7.3090 (3)		Okada & Ossaka (1980)
$NaK_3(SeO_4)_2$ (390 K)	5.906 (3)	5.906 (3)	7.552 (1)		Fábry *et al.* (1993)
$NaK_3(CrO_4)_2$	5.8580 (6)	5.8580 (6)	7.523 (2)		Madariaga & Breczewski (1990)
$NaK_3(CrO_4)_2$	5.857 (3)	5.857 (3)	7.521 (2)		Fábry *et al.* (1994)
Tl_2MoO_4 (350 K)	6.266 (1)	6.266 (1)	8.103 (2)		Friese *et al.* (1999)
Tl_2WO_4	6.278 (1)	6.278 (1)	8.099 (2)		Okada & Ossaka (1979)
Space group $C2/c$					
$Na_3Fe(PO_4)_2$	9.0637 (3)	5.0281 (2)	13.8581 (3)	91.434 (2)	Belkhiria *et al.* (1998)
$NaK_3(SeO_4)_2$	10.162 (2)	5.867 (1)	15.021 (2)	90.00 (1)	Fábry *et al.* (1993)
$NaK_3(CrO_4)_2$ (200 K)	10.117 (1)	5.843 (2)	15.024 (2)	89.97 (7)	Fábry *et al.* (1994)
$NaK_3(CrO_4)_2$ (230 K)	10.128 (3)	5.8437 (5)	15.0220 (2)	89.97 (2)	Fábry *et al.* (1994)
$NaK_3(MoO_4)_2$	10.4455 (14)	6.0307 (8)	15.240 (4)	90.00 (2)	Fábry *et al.* (1997)
Space group $C2/m$					
K_2MoO_4	12.348	6.081	7.538	115.74	Gatehouse & Leverett (1969*a*)
K_2WO_4	12.39 (1)	6.105 (5)	7.560 (5)	115.96 (3)	Koster *et al.* (1969)
Rb_2MoO_4	12.821 (2)	6.253 (1)	7.842 (1)	115.64 (1)	Kools *et al.* (1970)
Rb_2WO_4	12.841 (2)	6.285 (1)	7.854 (1)	115.82 (1)	Kools *et al.* (1970)
$(NH_4)_2SeO_4$	12.152 (6)	6.418 (3)	7.711 (4)	115.5 (1)	Carter *et al.* (1977)
$(NH_4)_2CrO_4$	12.30 (2)	6.294 (5)	7.664 (2)	115.6 (1)	Gatehouse & Leverett (1969*b*)
$(NH_4)_2CrO_4$	12.21 (1)	6.258 (3)	7.630 (4)	115.2 (2)	Stephens & Cruickshank (1970)
$(NH_4)_2MoO_4$ (228 K)	12.636 (3)	6.522 (14)	7.764 (2)	117.36 (1)	Dittmann & Schweda (1998)

the phase-matching condition $\Delta K = 0$ (*i.e.* $n_v^{2\omega} = n_h^{\omega}\theta$) is achieved for some θ.

The result for Tl_2MoO_4 is shown in Fig. 1. A broad peak with a maximum at $\sim 4^\circ$ from normal incidence is observed. The broadness of the peak is a consequence of the small thickness of the used sample. The interpretation of this peak as a consequence of the phase matching is in agreement with the fact that it was not observed when the fundamental light was vertically polarized, as in this case n_v^{ω} is constant and therefore the matching of indices is not possible.

It is clear that a complete characterization of the SHG properties of this material is not possible with such a small specimen like that employed in this work (the sample size was less than 10% of the laser beam diameter). However, an estimation of the second-harmonic conversion efficiency at phase matching leads to a value of $d_{\rm eff} = 5.5 \pm 0.5$ pm V^{-1}. This estimation was made from the maximum in $P^{2\omega}$ in Fig. 1 after a calibration of the experimental setup with a *y*-cut (*i.e.* normal to the [120] direction) quartz crystal ($d_{\rm eff} = d_{11} = 0.4$ pm V^{-1}). The obtained efficiency is similar to that exhibited by $LiNbO_4$ at the same wavelength ($d = 5.22$ pm V^{-1}) for the most favorable type I phase-matching situation (Dmitriev *et al.*, 1997).

3. X-ray diffraction and structure refinement

In the single-crystal X-ray diffraction experiments the frequent appearance of multiple domains in the room-temperature phase led to huge difficulties in the measurement of intensities. The orientation of the domains as observed in an optical microscope clearly indicates that the threefold axis of the high-temperature phase is the responsible twin element. Unfortunately, due to the deviation from the ideal hexagonal metrics, the reflections of the different domains do not superimpose exactly, but a slight splitting of reflections was observed. Thus, in a first intent, using a crystal with various domains we were not able to process the data which we recorded with an imaging plate. It was necessary to superimpose various lattices to index all the reflections and we did not succeed to obtain a sufficiently good separation of reflections originating from the different domains. Only when we mounted a very small crystal – a tiny, flat hexagonal prism (0.003 × 0.09 × 0.08 mm), where optically no domain structure was observed – was it possible to index all the reflections using one single lattice and no further experimental difficulties were encountered. Data collection was carried out with the Stoe IPDS at 293 K. Details concerning the data collection and refinement are given in Table 2. Of course, due to the shape of the crystal the absorption correction had a huge effect [the internal $R(F)$ value dropped from 0.124 to 0.057% after application of the absorption correction].

All reflections observed in the diffraction pattern can be indexed with the lattice parameters given in Table 2. The systematic extinctions observed are in agreement with a *C*-centered lattice leading to the possible space groups $C12/m1$, $C1m1$ or $C121$.

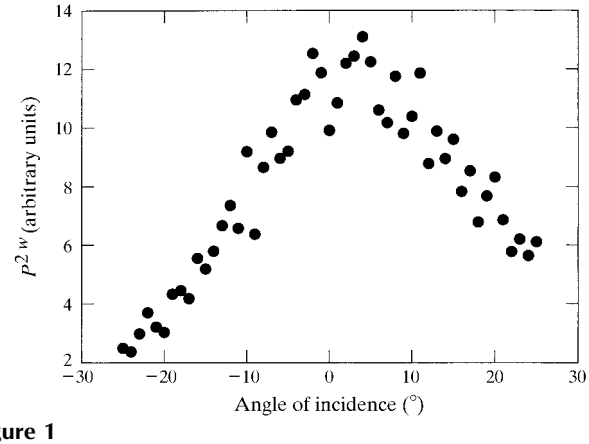

Figure 1
Second harmonic intensity (in arbitrary units) *versus* incident angle for Tl_2MoO_4 in the type I phase-matching experimental configuration: the fundamental field was horizontally polarized and the crystal was rotated about the vertical (twofold axis) direction. The maximum of the curve corresponds to the phase-matching condition.

Table 2
Experimental details.

Crystal data	
Chemical formula	MoO_4Tl_2
Chemical formula weight	568.68
Cell setting, space group	Monoclinic, *C*2
a, *b*, *c* (Å)	10.565 (3), 6.4178 (13), 8.039 (2)
β (°)	91.05 (4)
V (Å^3)	545.0 (3)
Z	4
D_x (Mg m^{-3})	6.931
Radiation type	Mo $K\alpha$
No. of reflections for cell parameters	1132
θ range (°)	2.53–25.92
μ (mm^{-1})	61.163
Temperature (K)	293 (2)
Crystal form, colour	Hexagonal prismatic, yellow
Crystal size (mm)	0.003 × 0.09 × 0.08
Data collection	
Diffractometer	Stoe IPDS
Absorption correction	Gaussian (Coppens, 1970)
T_{min}	0.0498
T_{max}	0.7962
No. of measured, independent and observed parameters	2138, 1006, 644
Criterion for observed reflections	$I > 2\sigma(I)$
R_{int}	0.0570
θ_{max} (°)	25.92
Range of *h*, *k*, *l*	$-12 \rightarrow h \rightarrow 12$ $-7 \rightarrow k \rightarrow 7$ $-9 \rightarrow l \rightarrow 9$
Refinement	
Refinement on	F^2
$R[F^2>2\sigma(F^2)]$, $wR(F^2)$, *S*	0.0285, 0.0388, 0.708
No. of reflections and parameters used in refinement	1006, 66
Weighting scheme	$w = 1/[\sigma^2(F_o^2) + (0.0000P)^2 + 0.0000P]$, where $P = (F_o^2 + 2F_c^2)/3$
$(\Delta/\sigma)_{max}$	0.001
$\Delta\rho_{max}$, $\Delta\rho_{min}$ (e Å^{-3})	0.961, −0.926
Extinction method	*SHELXL*97 (Sheldrick, 1997)
Extinction coefficient	0.00092 (4)

Computer programs used: Stoe IPDS software (Stoe & CIE, 1998), coordinates from model, *SHELXL*97 (Sheldrick, 1997).

Refinement was started from the transformed coordinates of the trigonal phase at 350 K using the program *SHELXL*97 (Sheldrick, 1997). As the SHG measurements clearly indicated that the crystal structure at room temperature is noncentrosymmetric we only tested the two noncentrosymmetric space groups. Refinement in space group *C*1*m*1 did not converge and thus we assumed the space group *C*121 to be the correct one.

The subgroup index $t = 6$ (t = translationengleich; Hermann, 1929) which corresponds to the phase transition ($P\bar{3}m1 \longrightarrow C121$; see Fig. 2) allows six possible orientations for different twin domains. We could easily exclude twinning *via* the threefold axis, as no splitting of reflections was observed. Anyhow, the treatment as an inversion twin led to a significant improvement of the *R* value, although the volume fraction of the second twin individual is comparatively small (about one sixth of the total volume).

Coordinates of the atoms and isotropic displacement parameters have been deposited.[1] Selected bond distances and angles are given in Table 3.

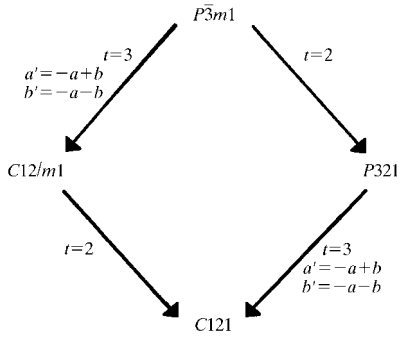

Figure 2
Group–subgroup graph for the high- and low-temperature phase of Tl_2MoO_4.

Table 3
Selected bond distances (Å) and angles (°) for Tl_2MoO_4 at 293 K.

Tl1—O4	2.73 (1) (2×)	Tl3—O1	2.56 (1)
Tl1—O3	2.79 (1) (2×)	Tl3—O3	2.78 (1)
Tl1—O2	2.94 (1) (2×)	Tl3—O4	2.92 (1)
Tl2—O2	2.75 (1) (2×)	Tl3—O2	2.94 (1)
Tl2—O3	3.07 (1) (2×)	Tl3—O4	3.31 (1)
Tl2—O4	3.09 (1) (2×)	Tl3—O4	3.41 (1)
Tl2—O1	3.26 (1) (2×)	Tl3—O2	3.49 (1)
Tl2—O1	3.33 (1) (2×)	Tl3—O3	3.49 (1)
		Tl3—O3	3.70 (1)
Mo—O2	1.70 (1)	O2—Mo—O3	109.9 (8)
Mo—O3	1.70 (1)	O2—Mo—O1	114.5 (7)
Mo—O1	1.72 (1)	O2—Mo—O4	105.1 (7)
Mo—O4	1.80 (1)	O3—Mo—O1	109.0 (7)
O1—O3	2.78 (2)	O3—Mo—O4	110.1 (7)
O1—O4	2.85 (2)	O1—Mo—O4	108.1 (7)
O1—O2	2.88 (2)		
O2—O3	2.79 (2)		
O2—O4	2.78 (2)		
O3—O4	2.87 (2)		

4. Symmetry mode analysis

To characterize the structural distortion involved in the phase transition we performed a symmetry mode analysis. A short outline of the procedure employed will be given here. For details the reader is referred to Pérez-Mato *et al.* (1986); applications can be found in Guelylah *et al.* (1996), Pérez-Mato *et al.* (1989) and Friese *et al.* (1999).

As mentioned before, *C*2 is a 'translationengleiche' subgroup of $P\bar{3}m1$ of index 6. Correspondingly, six different orientational domains are possible, of which, however, only two are realised in the studied specimen. We have therefore restricted our considerations to the *C*2-subgroup corresponding to the orientation of the monoclinic axes, which are in accordance with the experimental data (the transformation is given in Fig. 2), and we concentrate on the larger twin individual.

[1] Supplementary data for this paper are available from the IUCr electronic archives (Reference: NA0110). Services for accessing these data are described at the back of the journal.

Table 4
Character table for the irreducible representations of the group $\bar{3}m$.

$\bar{3}m$	1	3	2	$\bar{1}$	$\bar{3}$	m
A_{1g}	1	1	1	1	1	1
A_{2g}	1	1	−1	1	1	−1
E_g	2	−1	0	2	−1	0
A_{1u}	1	1	1	−1	−1	−1
A_{2u}	1	1	−1	−1	−1	1
E_u	2	−1	0	−2	1	0

The studied phase transition $P\bar{3}m1$–$C121$ is of displacive type. It can be attributed to the Γ point on the Brillouin zone and the corresponding **irreducible** representations (irreps) coincide with the irreps of the point group $\bar{3}m$ (see Table 4). The structural distortion relating the two phases can in general be decomposed into a homogeneous strain and an atomic displacement field, $u_\alpha(l, k)$ representing the displacements of each atom k in the unit cell l (α distinguishes the three independent components of the displacement vector). The displacement field $u_\alpha(l, k)$ is calculated from the difference of the atomic coordinates of the two structures in relative units. For our specific case $u_\alpha(l, k) \equiv u_\alpha(k)$ and the expression for the decomposition of the distortion in terms of symmetry modes is reduced to

$$u_\alpha(k) = \sum_\lambda A(\lambda)\epsilon_\alpha(k|\lambda). \tag{3}$$

Here, $\epsilon_\alpha(k|\lambda)$ and $A(\lambda)$ represent the polarization vector and the amplitudes for a given symmetry mode λ. The sum is over the symmetry modes compatible with the low-symmetry $C121$ structure. Two main types of symmetry modes are to be distinguished:

(i) Primary symmetry modes are the modes which contribute to the critical structural distortion. They transform according to the active representation related to the phase transition, *i.e.* the irrep to which the order parameter belongs. Its direction determines the so-called isotropy subgroup, which is exactly the group of the low-symmetry phase. For the $P\bar{3}m1$–$C2$ symmetry break, the two-dimensional E_u irrep (see Table 4) is the active one.

(ii) In general, apart from the critical primary distortion there are secondary distortions which also can have non-negligible contributions to the global structural distortion. As these distortions are compatible with the $C2$ symmetry, the symmetry modes associated with them transform according to $P\bar{3}m1$-irreps, whose corresponding isotropy groups contain $C2$ as a subgroup and are among the groups of the graph of maximal subgroups for the chain $P\bar{3}m1$–$C2$ (Fig. 2). Such irreps are A_{1g}, A_{1u}, E_g with $P\bar{3}m1$, $P321$ and $C2/m$ as isotropy subgroups, correspondingly.

The number of primary and secondary symmetry modes contributing to a structural distortion for the different orbits of symmetrically equivalent atoms follow from the decompositions of the corresponding vibrational representations into irreps of the high-symmetry group. In the case of Tl_2MoO_4 the atoms are distributed over four different Wyckoff positions and the corresponding decompositions are as follows:

$$1(a), 1(b) : \Gamma^{\rm vib}(a)(= \Gamma^{\rm vib}(b)) \sim A_{2u} \oplus E_u \tag{4}$$

$$2(d) : \Gamma^{\rm vib}(d) \sim A_{1g} \oplus A_{2u} \oplus E_u \oplus E_g \tag{5}$$

$$6(i) : \Gamma^{\rm vib}(i) \sim 2A_{1g} \oplus A_{2g} \oplus A_{1u} \oplus 2A_{2u} \oplus 3E_u \oplus 3E_g. \tag{6}$$

For example, the structural distortion for the set of 6(i)-symmetry related atoms can be decomposed into nine symmetry-mode contributions, three of which are primary (the remaining irreps A_{2u} and A_{2g} are not compatible with the symmetry $C2$ of the structural distortion).

The polarization-vector patterns of the symmetry modes are calculated using the group–subgroup relations of the space groups involved in the transition and the corresponding splittings of the occupied Wyckoff positions over the graph of maximal subgroups (for details on the method the reader is referred to Aroyo & Pérez-Mato, 1998). The obtained symmetry modes, also called chain-adapted modes in the following, are constructed and classified according to their compatability with the space groups in the subgroup chains of maximal subgroups. Clearly, this classification scheme is closely related to the isotropy-group classification mentioned above: the primary chain-adapted modes are compatible with the $C2$ symmetry, while the three types of the secondary modes correspond to the $P\bar{3}m1$, $P321$ and $C2/m$ symmetries. The chain-adapted modes for the different groups of atoms of Tl_2MoO_4 are given in Table 5. The coordinates of the atoms and the polarization vector patterns are listed with respect to the chosen orthohexagonal cell. The obtained modes are normalized with respect to the $C121$ unit cell.

There is just one primary mode for the Tl1 and Tl2 atoms occupying 1(a) and 1(b) Wyckoff positions of the $P\bar{3}m1$ phase and it is characterized by displacements along the monoclinic b axis [see (4)]. The contributions of three modes have to be considered for the decomposition of the distortion of the 2(d) atoms (Tl3, Mo, O1): one primary mode along the b axis and two secondary modes, compatible with $C2/m$ (along the a axis), and $P\bar{3}m1$ symmetry [along the c axis; see (5)]. In the case of O2 atoms occupying the 6(i) position (corresponding to O2, O3 and O4 in the low-symmetry phase), there are nine relevant modes: three primary ones and six secondary chain-adapted modes including two $P\bar{3}m1$ modes, three $C2/m$ modes and one $P321$ mode [(see (6)].

The listed chain-adapted modes are real and normalized. Due to their orthogonality properties

$$\sum_{k,\alpha} \epsilon_\alpha(k|\lambda')\epsilon_\alpha(k|\lambda) = \delta_{\lambda\lambda'} \tag{7}$$

the amplitudes of the modes $A(\lambda)$ in the total structural distortion are easy to determine

$$A(\lambda) = \sum_{k,\alpha} \epsilon_\alpha(k|\lambda)u_\alpha(k). \tag{8}$$

Table 5
Chain-adapted symmetry modes z compatible with the symmetry $C121$ for atoms at Wyckoff position 1(a) (0,0,0), 1(b) (0,0,1/2), 2(d) (1/3,2/3,z) and 6(i) (x, $\bar{x}$, z) of space group $P\bar{3}m$.

The coordinates of atoms and polarization vectors are given with respect to orthohexagonal cell ($x' = -05x_{tri} + 05y_{tri}$; $y' = -05x_{tri} - 05y_{tri}$; $z' = z_{tri}$; displacement vectors for atoms related by C-centering are identical and not given explicitly: the symmetry modes are normalized with respect to the $C121$ cell.

Atoms	Primary mode $\Phi_1(C2)$	Atoms	Primary mode $\Phi_2(C2)$	Atoms	Secondary modes $\Phi_3(P\bar{3}m1)$	Primary mode $\Phi_4(C2/m)$	$\Phi_5(C2)$
0,0,0	(0,1,0)	0,0,$\frac{1}{2}$	(0,1,0)	$\frac{1}{6}, \frac{1}{2}, z$	(0,0,1)	(1,0,0)	(0,1,0)
Factor	$\frac{1}{2}^{1/2}$	Factor	$\frac{1}{2}^{1/2}$	$-\frac{1}{6}, \frac{1}{2}, \bar{z}$	(0,0,$\bar{1}$)	($\bar{1}$,0,0)	(0,1,0)
				Factor	$\frac{1}{2}$	$\frac{1}{2}$	$\frac{1}{2}$

			Secondary modes						
Atoms	$\Phi_6(P\bar{3}m1)$	$\Phi_7(P\bar{3}m1$	$\Phi_8(P321)$	$\Phi_9(C2/m)$	$\Phi_{10}(C2/m)$	$\Phi_{11}(C2/m)$	$\Phi_{12}(C2)$	$\Phi_{13}(C2)$	$\Phi_{14}(C2)$
$\bar{x}, 0, z$	(−1, 0, 0)	(0, 0, 1)	(0, 1, 0)	(1, 0, 0)	(−1, 0, 0)	(0, 0, −1)	(0, 1, 0)	(0, 0, 0)	(0, 0, 0)
$\frac{1}{2}x, \frac{3}{2}\bar{x}, z$	$(\frac{1}{2}, -\frac{3}{2}, 0)$	(0, 0, 1)	$(-\frac{1}{2}, -\frac{1}{2}, 0)$	(1, 0, 0)	$(\frac{1}{2}, \frac{1}{2}, 0)$	$(0, 0, \frac{1}{2})$	$(\frac{1}{2}, \frac{1}{2}, 0)$	(−1, 1, 0)	(0, 0, 1)
$\frac{1}{2}x, \frac{3}{2}x, z$	$(\frac{1}{2}, \frac{3}{2}, 0)$	(0, 0, 1)	$(\frac{1}{2}, -\frac{1}{2}, 0)$	(1, 0, 0)	$(\frac{1}{2}, -\frac{1}{2}, 0)$	$(0, 0, \frac{1}{2})$	$(-\frac{1}{2}, \frac{1}{2}, 0)$	(1, 1, 0)	(0, 0, −1)
$x, 0, \bar{z}$	(1, 0, 0)	(0, 0, −1)	(0, 1, 0)	(−1, 0, 0)	(1, 0, 0)	(0, 0, 1)	(0, 1, 0)	(0, 0, 0)	(0, 0, 0)
$\frac{1}{2}\bar{x}, \frac{3}{2}\bar{x}, \bar{z}$	$(-\frac{1}{2}, -\frac{3}{2}, 0)$	(0, 0, −1)	$(\frac{1}{2}, -\frac{1}{2}, 0)$	(−1, 0, 0)	$(-\frac{1}{2}, \frac{1}{2}, 0)$	$(0, 0, -\frac{1}{2})$	$(-\frac{1}{2}, \frac{1}{2}, 0)$	(1, 1, 0)	(0, 0, −1)
$\frac{1}{2}\bar{x}, \frac{3}{2}x, \bar{z}$	$(-\frac{1}{2}, \frac{3}{2}, 0)$	(0, 0, −1)	$(-\frac{1}{2}, -\frac{1}{2}, 0)$	(−1, 0, 0)	$(-\frac{1}{2}, -\frac{1}{2}, 0)$	$(0, 0, -\frac{1}{2})$	$(\frac{1}{2}, \frac{1}{2}, 0)$	(−1, 1, 0)	(0, 0, 1)
Factor	$(1/24)^{1/2}$	$(1/12)^{1/2}$	$(1/8)^{1/2}$	$(1/12)^{1/2}$	$(1/8)^{1/2}$	$(1/6)^{1/2}$	$(1/8)^{1/2}$	$\frac{1}{4}$	$(1/8)^{1/2}$

The values of the amplitudes $A(\lambda)$ for all atoms are listed in Table 6. The results clearly show that for the Tl3, Mo and O1 atoms in position 2(d) the amplitudes of the primary mode have higher values than the secondary modes with a difference of up to an order of magnitude. The same happens for the O(2) modes along the c axis. However, it can also be observed that the amplitudes of the O(2)-secondary modes in the a, b plane are especially large and comparable to the contribution of the corresponding primary mode.

5. Comparison of the high- and low-temperature phase

Contrary to the literature which reports the room-temperature phase to be orthorhombic with space-group symmetry $Pnam$ or $Pna2_1$ (Gaultier & Pannetier, 1972; Sleight *et al.*, 1975), our investigations show that Tl_2MoO_4 at room temperature assumes the monoclinic space group $C121$. To our knowledge this space group has not been observed for any glaserite-related compound so far. The structural phase transitions of glaserite-related compounds which have been characterized in detail – namely the structures of $NaK_3(SeO_4)_2$ and $NaK_3(CrO_4)_2$ – both lead from the trigonal space group $P\bar{3}m1$ to the monoclinic space group $C2/c$ and involve (apart from the change to the orthogonal setting) a doubling of the c axis. In these two compounds as well as in $NaK_3(MoO_4)_2$, which also crystallizes in $C12/c$, the ratio a/b is still very close to the ideal value of $3^{1/2}$. In Tl_2MoO_4, on the other hand, the b axis is significantly lengthened with respect to a in contrast to the compound $Na_3Fe(PO_4)_2$, where the a/b ratio is higher [Tl_2MoO_4: $a/b = 1.646$; $Na_3Fe(PO_4)_2$: $a/b = 1.803$].

The most important change observed in the structure of Tl_2MoO_4 can be easiest described as a rotation of the $[MoO_4]^{2-}$ tetrahedra around the hexagonal a (or b) axis (see Fig. 3). The average Mo—O distances within the tetrahedra do not differ significantly in the two phases [$< T - O >_{350}$ = 1.72 (1) Å; $< T - O >_{293}$ = 1.73 (1) Å]. Yet the Mo—O distances in the high-temperature phase are 1.70 (2) Å (O1) and 1.73 (2) Å (O2) in comparison to 1.70 (1) and 1.80 (1) Å in the low-temperature phase. Tetrahedral edge lengths at 350 K are 2.78 (2)–2.83 (2) Å, while at 293 K they range from 2.75 (2) to 2.88 (2) Å. The angles vary from 107.6 (4) to 111.3 (4)° in the trigonal phase and range from from 105.1 (7) to 114.5 (7)° in the monoclinic phase. Consequently, the values of the bond length distortion parameter (BLDP) and the edge length distortion parameter (ELDP; see Table 7; for details see Griffen & Ribbe, 1976) increase in the low-temperature phase, indicating the higher distortion of the tetrahedra.

The above-mentioned rotation of the tetrahedra leads to a considerable change in the coordination sphere of the three Tl atoms (see Fig. 4). The nearly regular $[Tl1O_6]^{11-}$ octahedra of the high-temperature phase is strongly distorted in the low-temperature phase. In the high-temperature phase all of the Tl1—O distances are equal [2.77 (1) Å], while at 293 K the distances are 2.73 (1), 2.79 (1) and 2.94 (1) Å; the mean Tl1—O distance is 2.82 (1) Å, which is slightly increased in the monoclinic phase.

For the other two Tl atoms the change in coordination is even more drastic. For Tl2 the coordination number decreases

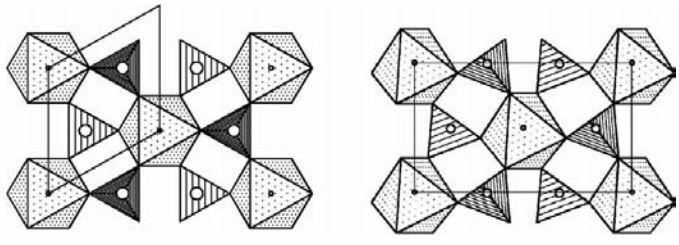

Figure 3
a,*b* projections of the structure of Tl_2MoO_4 at (*a*) 350 K and (*b*) 293 K. Molybdate tetrahedra and octahedra around Tl are shown (drawn using *STRUPLO*; Fischer, 1985).

Table 6
Amplitudes $\times 10^4$ of the symmetry modes for the symmetry break $P\bar{3}m1 > C121$ for Tl_2MoO_4; amplitudes given in relative units.

Atom	Φ_1 (C2)	Φ_2 (C2)	Φ_3 ($P\bar{3}m1$)	Φ_4 ($C2/m$)	Φ_5 ($C2$)
Tl1	273				
Tl2		−442			
Tl3			79	5	245
Mo			82	87	−127
O1			242	−489	1407

Atom	Φ_6 ($P\bar{3}m1$)	Φ_7 ($P\bar{3}m1$)Φ_8 ($P321$)	Φ_8 ($P321$)	Φ_9 ($C2/m$)	Φ_{10} ($C2/m$)	Φ_{11} ($C2/m$)	Φ_{12} ($C2$)	Φ_{13} ($C2$)	Φ_{14} ($C2$)
O2	−267	3	−939	589	290	−446	−777	−305	−1225

Table 7
Comparison of some selected data for the high-temperature phase of Tl_2MoO_4 at 350 (Friese *et al.*, 1999) and 293 K.

Distortion parameters of the tetrahedra according to

$$\mathrm{BLDP} = (1/\langle T-O\rangle)\sum_{i=1}^{4}[((T-O)_i - \langle T-O\rangle)^2]^{1/2}/3;$$

$$\mathrm{ELDP} = (1/\langle O-O\rangle)\sum_{i=1}^{6}[((O-O)_i - \langle O-O\rangle)^2]^{1/2}/3$$

with $\langle T-O\rangle$ = average bond distance; $(T-O)_i$ = individual bond distance; $\langle O-O\rangle$ = average edge length; $(O-O)_i$ = individual edge length. BVS = bond-valence sums according to Brese & O'Keefe (1991).

	293 K	350 K
Space group	$C121$	$P\bar{3}m$
a (Å)	10.565 (3)	6.266 (1)
b (Å)	6.418 (1)	6.266 (1)
c (Å)	8.039 (2)	8.103 (2)
β (°)	91.05 (4)	
V (Å^3)	545.0 (4)	275.52 (9)
BVS Tl1 (v.u.)	1.08	1.20
BVS Tl2 (v.u.)	0.96	0.87
BVS Tl3 (v.u.)	0.96	0.90
BVS Mo (v.u.)	6.49	6.66
$\langle$Mo − O$\rangle$ (Å)	1.73 (1)	1.72 (1)
BLDP $\times 10^{-3}$	15.4	6.7
ELDP $\times 10^{-3}$	11.9	7.3
$\langle$Tl1 − O$\rangle$ (Å)	2.82 (1)	2.77 (1)
Coordination number Tl1	6	6
Coordination number Tl2	10	12
Coordination number Tl3	9	10

from 12 to 10, for Tl3 it is changed from 10 to 9 (see Fig. 4). The shortest Tl2—O distance is decreased from 2.94 (1) Å in the trigonal phase to 2.75 (1) Å in the monoclinic phase. On the other hand, the shortest Tl—O distance [Tl3—O: 2.47 (2) Å] in the high-temperature phase is lengthened to 2.56 (1) Å in the low-temperature phase.

The bond-valence sums calculated according to Brese & O'Keefe (1991) reaching the cations in the low-temperature phase are slightly closer to the ideal values compared to the high-temperature phase. Thus, the valence sums for the three Tl atoms change from 1.20, 0.87 and 0.90 v.u. (Friese *et al.*, 1999) to 1.08, 0.96 and 0.96 v.u. in the low-temperature phase. The bond-valence sums reaching the molybdenum ion change from 6.66 to 6.49 v.u. (see Table 7).

The connection between the Tl polyhedra and the tetrahedra also suffers a very important change. In the high-temperature phase the Tl2 polyhedra share six common edges with the $[MoO_4]^{2-}$ tetrahedra, which correspond to the shortest O—O edges within the polyhedra [6 × 2.83 2) Å]. In the low-temperature phase the number of common edges between the Tl2 polyhedra and the tetrahedra is reduced to four with O—O distances of 2.78 (2) (2×) and 2.85 (2) Å (2×). The Tl3 polyhedra in the high-temperature phase share one common face (O2—O2—O2) with the tetrahedra [O2—O2 3× 2.78 (2) Å] and have in addition three common edges with the tetrahedra [O1—O2 2.83 (2) Å]. In the low-temperature phase the common face is changed into a common edge [O3—O4 2.87 (2) Å], while the three common edges are retained [O2—O3 2.79 (2), O2—O4 2.78 (2), O3—O4 2.87 (2) Å].

According to the third rule of Pauling (1959), common edges between polyhedra and especially common faces reduce the stability of a compound. Furthermore, in this case, contrary to the fourth rule of Pauling, the tetrahedra formed around the cation of high valence is involved in the face sharing. From the viewpoint of crystal chemistry this is most probably the reason for the instability of the high-temperature phase and the ensuing phase transition.

To obtain a clearer idea of the structural changes brought about by the different symmetry modes and especially to reach a better understanding of the presumably dominant role of the primary symmetry modes, we calculated a series of hypothetical structures. In these we took into account just the contributions of part of the symmetry modes. For example, to calculate the hypothetical Tl_2MoO_4 structure with symmetry $P321$ we substracted from the coordinates of the atoms in the high-symmetry phase the contributions of the modes compatible with this symmetry.[2]

In detail, the contributions taken into account for the different hypothetical structures are the following

$$\Phi_3 + \Phi_6 + \Phi_7 \longrightarrow \text{ for symmetry } P\bar{3}m1$$

$$\Phi_3 + \Phi_6 + \Phi_7 + \Phi_8 \longrightarrow \text{ for trigonal symmetry } (P321 + P\bar{3}m1)$$

$$\Phi_4 + \Phi_9 + \Phi_{10} + \Phi_{11} \longrightarrow \text{ for symmetry } C12/m1$$

[2] The amplitudes of the modes have been calculated subtracting the relative coordinates of the low-symmetry phase from the corresponding coordinates of the high-symmetry phase.

Table 8
Bond-valence sums according to Brese & O'Keeffe (1991) for the real and hypothetical structures of Tl_2MoO_4 Hypothetical structures were calculated taking into account only the contribution of symmetry modes compatible with the given symmetry.

Atom	350 K $P\bar{3}m1$	293 K $C121$	$P\bar{3}m1$	$P\bar{3}m1 + P321$	$C12/m1$	Secondary modes	$C121$
Tl1	1.20	1.08	1.07	1.04	1.29	1.13	1.17
Tl2	0.87	0.96	0.79	0.78	0.99	0.89	1.03
Tl3	0.90	0.96	0.82	0.88	0.94	0.95	0.95
Mo	6.66	6.49	7.97	7.77	6.15	7.16	6.18

$$\Phi_3+\Phi_4+\Phi_6+\Phi_7+\Phi_8+\Phi_9+\Phi_{10}+\Phi_{11}\longrightarrow$$
structure considering all secondary modes

$$\Phi_1+\Phi_2+\Phi_5+\Phi_{12}+\Phi_{13}+\Phi_{14}\longrightarrow$$
structure considering all primary modes.

Using the relative coordinates obtained this way we calculated interatomic distances and bond-valence sums. For this we used the lattice parameters of the high-temperature phase for the structures involving modes compatible with trigonal symmetry, while for the hypothetical structures with monoclinic symmetry we used the lattice parameters of the $C121$ phase.

Table 8 gives the calculated bond-valence sums of the cations. As can be clearly seen, the two hypothetical structures with trigonal symmetry lead to rather poor bond-valence sums for Tl2, Tl3 and especially Mo. The hypothetical structure with symmetry $C12/m1$, on the other hand, gives good values for these atoms, but leads to the high valence of 1.29 for Tl1. The hypothetical structure which takes into account all secondary symmetry modes also does not give very satisfying results.

Yet, the hypothetical structure with symmetry $C121$, taking into account only the primary modes, gives remarkably good results for all cations. In fact, for all atoms apart from Tl1 the calculated values are even better than in the real structure. A refinement using the relative coordinates of this hypothetical structure in which we allowed the displacement factors of the atoms to be varied already leads to an $R(F)_{obs}$ value of approximately 0.05 for the data of the low-temperature phase [the value obtained for $R(F)_{obs}$ for the real structure is 0.029]. Anyhow, one clearly observes the contribution of the secondary modes in the anisotropic displacement factors.

Given the reasonable results when only the primary modes are taken into account, it is not clear why the secondary modes play such a relatively important role in the structural change. Considering the bond valences it is obvious that only the Tl1 atom gains in the real structure when compared to the hypothetical structure calculated using only the primary modes. The secondary modes with trigonal symmetry seem to influence the bond-valence sums of this atom rather positively and this probably makes them of some importance. Maybe the secondary modes of symmetry $C2/m$ are then necessary to counterbalance the effect of the trigonal modes on the bond valences of Tl2, Tl3 and Mo.

As far as the coordination numbers and the connections of the different polyhedra are concerned, all of the hypothetical structures calculated on the basis of only secondary modes do not change the coordination polyhedra of the Tl atoms, as found in the high-temperature phase. Furthermore, they also leave the common face between the Tl3 polyhedra and the Mo tetrahedra, which is observed in the high-temperature phase basically untouched.

The primary modes, on the other hand, change the coordination around the Tl atoms and lead to polyhedra comparable to those observed in the low-symmetry phase. More important is the fact that they lead to structural changes which result in an elimination of the disadvantageous face sharing.

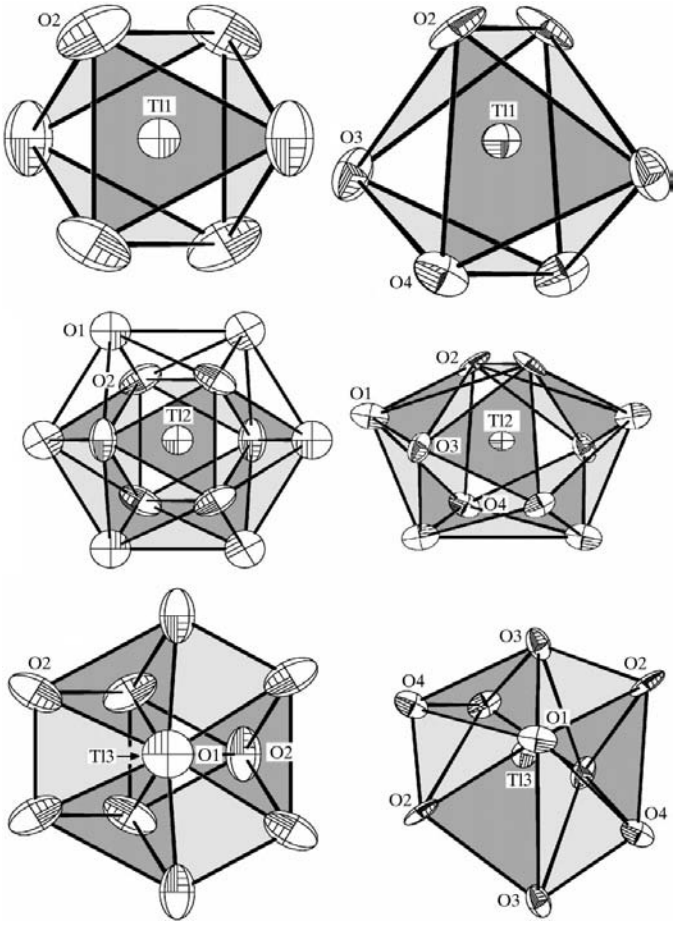

Figure 4
The three different Tl coordination polyhedra in Tl_2MoO_4 (*a*) at 350 K and (*b*) at 293 K. Projections onto the *a*,*b* plane; drawn with *ORTEP*3 (Farrugia, 1996).

The authors gratefully acknowledge financial support by the Universidad del País Vasco (EB098/97), the Gobierno Vasco (PI97/71) and the Deutsche Forschungsgemeinschaft (Fr1332/2–1).

References

Akker, A. W. M. van den, Koster, A. & Rieck, G. D. (1970). *J. Appl. Cryst.* **3**, 389–392.

Aroyo, M. & Pérez-Mato, J. M. (1998). *Acta Cryst.* A**54**, 19–30.

Belkhiria, M. S., Laaribi, S., Ben'Hadj'Amara, A. & Ben'Amara, M. (1998). *Ann. Chim. (Paris)*, **23**, 117–120.

Berg, A. J. van den, Overeijnder, H. & Tuinstra, F. (1983). *Acta Cryst.* C**39**, 678–680.

Berg, A. J. van den, Tuinstra, F. & Warczewski, J. (1973). *Acta Cryst.* B**29**, 586–589.

Brese, N. E. & O'Keeffe, M. (1991). *Acta Cryst.* B**47**, 192–197.

Carter, R., Koerntgen, C. & Margulis, T. (1977). *Acta Cryst.* B**33**, 592–593.

Coppens, P. (1970). *Crystallographic Computing*, edited by F. R. Ahmed, S. R. Hall & C. P. Huber, pp. 255–270. Copenhagen: Munksgaard.

Dittmann, M. & Schweda, E. (1998). *Z. Anorg. Allg. Chem.* **624**, 2033–2037.

Dmitriev, V. G., Gurzadyan, G. G. & Nikogosyan, D. N. (1997). *Handbook of Nonlinear Optical Crystals.* Berlin: Springer-Verlag.

Fábry, J., Breczewski, T. & Madariaga, G. (1994). *Acta Cryst.* B**50**, 13–22.

Fábry, J., Breczewski, T. & Petrícek, V. (1993). *Acta Cryst.* B**49**, 826–832.

Fábry, J., Petrícek, V., Vanek, P. & Císarová, I. (1997). *Acta Cryst.* B**53**, 596–603.

Farrugia, L. J. (1996). *ORTEP*3 *for Windows.* University of Glasgow, Scotland.

Fischer, R. X. (1985). *J. Appl. Cryst.* **18**, 258–262.

Friese, K., Madariaga, G. & Breczewski, T. (1999). *Acta Cryst.* C**55**, 1753–1755.

Gatehouse, B. M. & Leverett, P. (1969*a*). *J. Chem. Soc. A: Inorg. Phys. Theoret.* pp. 849–854.

Gatehouse, B. M. & Leverett, P. (1969*b*). *J. Chem. Soc. A: Inorg. Phys. Theoret.* pp. 1857–1861.

Gaultier, M. & Pannetier, G. (1972). *Rev. Chim. Miner.* **9**, 271–289.

Griffen, D. T. & Ribbe, P. H. (1976). *N. Jahrb. Miner. Abh.* **137**, 54–73.

Guelylah, A., Aroyo, M. I. & Pérez-Mato, J. M. (1996). *Phase Transit.* **59**, 155–179.

Hermann, C. (1929). *Z. Kristallogr.* **69**, 533–555.

Kools, F. X. N. M., Koster, A. S. & Rieck, G. D. (1970). *Acta Cryst.* B**26**, 1974–1977.

Koster, A. S., Kools, F. X. N. M. & Rieck, G. D. (1969). *Acta Cryst.* B**25**, 1704–1708.

Madariaga, G. & Breczewski, T. (1990). *Acta Cryst.* C**46**, 2019–2021.

Mandarino, J. A. (1976). *Can. Mineral.* **14**, 498–502.

Mandarino, J. A. (1978). *Can. Mineral.* **16**, 169–174.

Moore, P. B. (1973). *Am. Mineral.* **58**, 32–42.

Okada, K. & Ossaka, J. (1979). *Acta Cryst.* B**35**, 2189–2191.

Okada, K. & Ossaka, J. (1980). *Acta Cryst.* B**36**, 919–921.

Pauling, L. (1959). *The Nature of the Chemical Bond.* Ithaca: Cornell University Press.

Pereda, N., Folcia, C. L., Etxebarria, J., Ortega, J. & Ros, M. B. (1998). *Liq. Cryst.* **24**, 451–456.

Pérez-Mato, J. M., Gaztelua, F., Madariaga, G. & Tello, M. J. (1986). *J. Phys. C*, **19**, 1923–1935.

Pérez-Mato, J. M., Zúniga, F. J. & Madariaga, G. (1989). *Phase Transit.* **16/17**, 439–444.

Pontonnier, L., Caillet, M. & Aleonard, S. (1972). *Mater. Res. Bull.* **7**, 799–812.

Sheldrick, G. (1997). *SHELXL*97. University of Karlsruhe, Germany.

Sleight, A. W., Bierlein, J. D. & Bierstedt, P. E. (1975). *J. Chem. Phys.* **44**, 2826–2827.

Stephens, J. S. & Cruickshank, D. W. J. (1970). *Acta Cryst.* B**26**, 437–439.

Stoe & CIE (1998). *X-RED.* Stoe and CIE GmbH, Darmstadt, Germany.

Yariv, A. & Yeh, P. (1984). *Optical Waves in Crystals.* John Wiley and Sons.